



Performance of liver surface nodularity quantification for the diagnosis of portal hypertension in patients with cirrhosis: comparison between MRI with hepatobiliary phase sequences and CT

Nicolas De Vos^{1,2} · Riccardo Sartoris¹ · François Cauchy¹ · Pierre-Emmanuel Rautou¹ · Valérie Vilgrain¹ · Maxime Ronot¹

Published online: 3 December 2019
© Springer Science+Business Media, LLC, part of Springer Nature 2019

Abstract

Purpose To assess and compare the performance of liver surface nodularity (LSN) quantification using Gd-BOPTA-enhanced MRI and contrast-enhanced CT for the diagnosis of clinically significant portal hypertension (CSPH) in patients with cirrhosis.

Methods This retrospective study included 30 patients with compensated histologically proven cirrhosis who underwent hepatic venous pressure gradient (HVPG), abdominal CT and Gd-BOPTA-MRI within a 60-day interval during pre-surgery workup for hepatocellular carcinoma (HCC) between January 2016 and August 2018. LSN score was derived from CT portal venous phase (PVP), axial T2- and T1-weighted PVP and hepatobiliary phase (HBP). Accuracy for the detection of CSPH was evaluated for each set of images by ROC curve analysis. Intra-observer, inter-observer and inter-method reproducibilities were assessed by the intraclass correlation coefficient (ICC) and coefficient of variation (CV).

Results Thirty patients were analysed (23 men [77%], mean age 60 ± 11 years old), including 15 (50%) with CSPH. All CT- and MRI-derived LSN quantifications were correlated to HVPG (CT-PVP: $r = 0.63$, $p = 0.001$, AUROC = 0.908 ± 0.06 ; T1-w-PVP: $r = 0.43$, $p = 0.028$, AUROC = 0.876 ± 0.07 ; T1-w-HBP: $r = 0.50$, $p = 0.012$, AUROC = 0.823 ± 0.08 ; T2-w: $r = 0.51$, $p = 0.007$, AUROC = 0.801 ± 0.09). There was no significant difference in AUROC pairwise comparisons ($p = 0.12$ – 0.88). Patients with CSPH had higher LSN than those without (CT-PVP: 3.2 ± 0.6 vs 2.4 ± 0.5 , $p < 0.001$; T1-w-PVP: 2.7 ± 0.4 vs 2.2 ± 0.4 , $p = 0.002$; T1-w-HBP: 3.0 ± 0.6 vs 2.3 ± 0.3 , $p < 0.001$; T2-w: 3.0 ± 0.6 vs 2.2 ± 0.3 , $p = 0.001$) and 86%, 82%, 85% and 82% of patients were correctly classified, respectively. Reproducibility of inter-image set comparisons was excellent (ICC = 0.84 – 0.96 and CV = 8.3 – 14.2%).

Conclusion The diagnostic performance of MRI-based LSN for detecting CSPH is strong and similar to that of CT-based LSN.

Keywords Cirrhosis · Non-invasive · Nodularity · Portal hypertension

Electronic supplementary material The online version of this article (<https://doi.org/10.1007/s00261-019-02355-y>) contains supplementary material, which is available to authorised users.

✉ Maxime Ronot
ronot.maxime@aphp.fr

Nicolas De Vos
nicdvos.devos@ugent.be

Riccardo Sartoris
riccardo.sartoris@aphp.fr

François Cauchy
francois.cauchy@aphp.fr

Pierre-Emmanuel Rautou
pierre-emmanuel.rautou@bjn.aphp.fr

Valérie Vilgrain
valerie.vilgrain@aphp.fr

¹ Department of Radiology, APHP, University Hospitals Paris Nord Val de Seine, Beaujon, 100 Boulevard du Général Leclerc, 92110 Clichy, France

² Department of Radiology, Ghent University Hospital, Corneel Heymanslaan 10, 9000 Ghent, Belgium

Introduction

Portal hypertension plays a role in most of the complications of liver cirrhosis, for example gastroesophageal variceal bleeding, and is a major risk factor for mortality. Portal hypertension has also been shown to be correlated with morbidity and mortality in patients with cirrhosis who undergo major liver surgery [1, 2]. The reference standard to evaluate the presence and severity of portal hypertension in patients with cirrhosis is the hepatic venous pressure gradient (HVPG) and clinically significant portal hypertension (CSPH) is defined as a HVPG ≥ 10 mmHg [3]. Even though HVPG measurement is a safe and minimally invasive procedure with low complication rate, it is only available in expert centres [4].

Non-invasive methods have been developed for the quantification of portal hypertension and the detection of CSPH in patients with cirrhosis, in particular liver stiffness assessed by transient elastography and derived scores [5]. Although liver stiffness can accurately exclude the presence of high-risk varices, [6] it is limited by the need for specific equipment and it can be difficult to perform in obese patients. Liver and spleen stiffness by shear-wave elastography has been found to be a promising approach but the diagnostic accuracy of this technique is not sufficient to estimate CSPH [7]. Several studies have also evaluated various MRI-derived parameters as possible surrogate markers for HVPG, but these techniques have not yet been validated and often require advanced MR sequences or MR elastography [8–10].

A software tool has been developed that retrospectively quantifies liver surface nodularity (LSN) based on routine computed tomography (CT). This approach which provides quantitative measurement of liver margin irregularities, a well-known feature of cirrhosis, has been validated in several studies for the evaluation of liver fibrosis and has also been shown to be accurate for the diagnosis of CSPH in patients with compensated cirrhosis [11–14]. This LSN software has also been recently applied to magnetic resonance imaging (MRI) for the detection of cirrhosis and has shown to have good agreement with CT-based LSN scores [15].

Because of the widespread use of MRI in the pre-surgical workup of patients with cirrhosis and hepatocellular carcinoma, and the use of liver-specific MR contrast agents especially during the hepatobiliary phase (HBP) [16], the goal of this study was to evaluate and compare the diagnostic performance of an MRI-based LSN score with different sequences to the CT-based LSN score for the diagnosis of CSPH in patients with cirrhosis, using HVPG measurement as the reference method.

Methods

Patient population

This retrospective single centre study as well as the protocol review was approved by the institutional review board and the requirement for written informed consent was waived. The study cohort included 177 consecutive patients between January 2016 and August 2018, with histologically proven cirrhosis and no previous hepatic interventions (such as transjugular intrahepatic portosystemic shunts, liver transplantation or liver resection). All patients underwent a HVPG measurement during a pre-surgical workup for hepatocellular carcinoma (HCC) including contrast-enhanced CT and gadobenic acid (Gd-BOPTA)-enhanced MRI examinations within a 60-day interval. The choice of the 60 days cutoff was chosen to limit the risk of portal hypertension variation between HVPG measurement and MR imaging. Diagnosis of cirrhosis was confirmed by liver biopsy performed before or during the HVPG measurement and the diagnosis of hepatocellular carcinoma was obtained by biopsy or in the resected specimen after surgery. Exclusion criteria were no contrast-enhanced CT or Gd-BOPTA-MRI within 60 days before or after the HVPG measurement (145 patients) and liver surgery performed between the CT and MRI examinations (left hepatectomy in 1 patient). An additional patient was excluded due to portal thrombosis detected on CT. Thus, the final population included 30 patients [mean age \pm standard deviation, (range) 60 ± 11 years old, (23–76)], including 23 (77%) men (61 ± 12 years old, (29–76)) and 7 (23%) women [58 ± 12 years old, (54–74)]. Flowchart of the study is showed in Supplementary Material.

HVPG measurement

HVPG measurements were performed under local anaesthesia. A catheter was introduced using the Seldinger technique, then a 7 French balloon catheter was inflated in the right or median hepatic vein to measure the wedged hepatic venous pressure. Occlusion was then confirmed by injection of 5 mL of iodinated contrast. Free hepatic venous pressure was then obtained. Finally, the HVPG was calculated as the difference between the wedged and free hepatic venous pressures.

CT acquisition

Abdominal contrast-enhanced CT was performed within 60 days before or after HVPG measurements and before liver surgery on a 256-section multidetector CT scanner (GE LightSpeed VCT; GE Healthcare, Milwaukee, Wisconsin, USA) with contrast-enhanced acquisitions following

intravenous administration of 2 mL/kg of a non-ionic contrast medium at 350 mg iodine/mL with a power injector, through an 18-gauge catheter at a rate of 4 mL/s. Portal venous phase (PVP) images were obtained 70 s after the beginning of contrast administration.

MRI acquisition

MRI was performed with a 3.0 T MRI scanner (Achieva; Philips Healthcare, Best, The Netherlands) equipped with high performance gradients and an 8-channel phased array coils.

The standard liver MR protocol included a fat-suppressed T2-weighted (T2-w) fast spin-echo sequence, a T2-w single-shot fast spin-echo sequence, a 3b-diffusion-weighted sequence and a transverse breath-hold 3D T1-weighted (T1-w) fat-suppressed spoiled gradient-recalled echo sequence before and after dynamic injection of contrast medium. The sequences used for LSN quantification were: T2-w single-shot fast spin-echo, T1-w-PVP and T1-w-HBP because of the high liver-fat contrast. A total of 0.05 mmol/kg of body weight of Gd-BOPTA followed by a 20 mL saline solution flush were administered at 2 and 1 mL/s, respectively with a power injector. Triple arterial, portal and delayed sequences were obtained. HBP images were acquired 2 h after contrast administration. CT and MRI technical data are provided in Supplemental Tables 1 and 2.

LSN score

Customised semi-automated LSN software (Liver Surface Nodularity Software, version 0.88; Liver Nodularity LLC) was applied to both CT and MRI examinations by two independent observers (observer 1, with 4 years of experience and observer 2, with 7 years of experience) blinded to

clinical data. To test intra-observer variability, observer 1 repeated the evaluation after a six-week interval and was blinded to the prior results of clinical data.

A region of interest of 1–2 cm in diameter was drawn along the liver surface of liver on different slices. The distance between the detected liver edge and the software-generated polynomial line was automatically measured on a pixel-by-pixel basis [15]. Measurements were obtained for each patient on CT-PVP and on T2-w, T1-w-PVP and T1-w-HBP MR sequences. Based on previous studies, measurements were obtained along the anterior aspect of the left liver lobe and segment 4 [11, 17]. Surfaces of the liver other than those mentioned above, regions where the liver contacted the abdominal wall, natural turns or fissures of the liver and the liver dome were avoided.

The images were confirmed by the observer after the measurements had been obtained to ensure that the imaging software had not visualised turns that did not seem to correspond to the liver surface, and any measurements that did not correspond to the liver surface were rejected and were not included in the final LSN score. Ten measurements were accepted for each series of images, according to previous studies [12, 15]. The final LSN score was automatically calculated by the software as the arithmetical mean of the ten slices measured, with a higher LSN score corresponding to a higher degree of surface nodularity. Failure was defined when ten measurements could not be obtained [12, 15]. Data were automatically recorded by software. Figure 1 shows examples of LSN measurements.

Statistical analysis

Continuous variables were expressed as means and standard deviations and compared using the Student *t* test or Mann–Whitney test whenever appropriate. Correlations

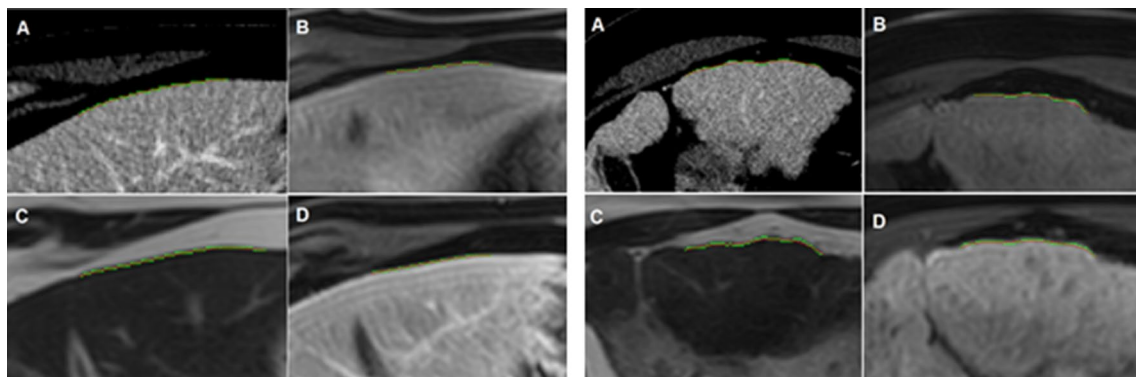


Fig. 1 LSN measurements in patients without clinically significant portal hypertension (CSPH) and with CSPH. Left: 43-year-old male patient with hepatitis C cirrhosis and a hepatic venous portal gradient (HVPG) measurement of 7 mmHg. **a** CT with LSN 2.21; **b** MRI T1-w-HBP with LSN 2.15; **c** MRI T2-w with LSN 2.33; **d** MRI

T1-w-PVP with LSN 2.28. Right: 62-year-old male patient with hepatitis C cirrhosis and HVPG measurement of 17 mmHg. **a** CT with LSN 3.95; **b** MRI T1-w-HBP with LSN 4.32; **c** MRI T2-w with LSN 4.07; **d** MRI T1-w-PVP with LSN 3.96

were determined with the Spearman correlation coefficient. The discriminative value for the identification of CSPH was assessed by measuring the area under the receiver operating characteristic (AUROC) curve provided with the corresponding standard deviation. Optimal cutoff values were identified with the Youden index and associated sensitivities, specificities, and positive and negative predictive values were determined. Comparison of AUROCs was performed using the DeLong method. Variability among the different LSN scores was assessed for each patient with the coefficient of variation (CV). Intra-reader and inter-reader variabilities were assessed with the intraclass correlation coefficient (ICC) and Bland–Altman plot. All tests were two-sided and 0.05 was considered to be statistically significant. Statistical analyses and figures were obtained with SPSS statistical package software (version 24.0; SPSS, Chicago, Illinois, USA) and GraphPad Prism software (version 7; GraphPad Software, La Jolla, California, USA), respectively.

Results

Study population

Fifteen (50%) of the 30 included patients had CSPH.

Cirrhosis was caused by alcohol consumption in 12 patients (40%), hepatitis C virus infection in 9 (30%), non-alcoholic fatty liver disease in 7 (23%), hepatitis B virus infection in 6 (20%) and other causes in 4 patients (13%) (the total exceeds 100% because some patients had more than one cause of cirrhosis). Patient characteristics are presented in Table 1.

Feasibility of LSN measurements

No reliable LSN measurements were possible on any MRI or CT acquisitions in one patient due to a limited liver-adipose tissue interface. Due to a limited liver-adipose tissue interface and limited amount of ascites, no reliable LSN

Table 1 Study population characteristics

| Characteristics | All patients (n = 30) | No CSPH (n = 15) | CSPH (n = 15) | P value |
|---------------------------------------|-----------------------|------------------|-----------------|---------|
| Men | 23 (77) | 12 (80) | 11 (73) | 0.66 |
| Age (years) ^b | | | | |
| Overall | 60 ± 11 (29–76) | 60 ± 14 (29–76) | 60 ± 8 (44–73) | 1.00 |
| Men | 59 ± 12 (29–76) | 57 ± 15 (29–76) | 60 ± 8 (44–70) | 0.56 |
| Women | 66 ± 8 (54–74) | 70 ± 4 (65–74) | 61 ± 10 (54–73) | 0.21 |
| Body Mass Index (kg/m ²) | 28 ± 6 | 28 ± 6 | 28 ± 7 | 1.00 |
| Cause of Cirrhosis ^{a, c} | | | | |
| Hepatitis C virus infection | 9 (30) | 6 (40) | 3 (20) | 0.24 |
| Hepatitis B virus infection | 6 (20) | 4 (27) | 2 (13) | 0.35 |
| Alcohol consumption | 12 (40) | 4 (27) | 8 (53) | 0.15 |
| Non-alcoholic fatty liver disease | 7 (23) | 2 (13) | 5 (33) | 0.20 |
| Other | 4 (13) | 2 (13) | 2 (13) | 1.00 |
| Days between HVPG and CT | 16.5 ± 17.0 | 18.5 ± 18.0 | 14.5 ± 17.1 | 0.54 |
| Days between HVPG and MRI | 21.7 ± 18.5 | 21.1 ± 16.7 | 22.4 ± 21.4 | 0.85 |
| Days between CT and MRI | 22.3 ± 22.9 | 28.7 ± 23.6 | 16.9 ± 22.8 | 0.17 |
| HVPG (mm Hg) | 10 ± 5 | 5 ± 2 | 14 ± 3 | < 0.001 |
| Platelet count (× 10 ⁹ /L) | 171 ± 60 | 174 ± 63 | 167 ± 60 | 0.75 |
| LSN MRI T1-w-PVP | 2.4 ± 0.4 | 2.2 ± 0.4 | 2.7 ± 0.4 | 0.002 |
| LSN MRI T1-w-HBP | 2.6 ± 0.6 | 2.3 ± 0.3 | 3.0 ± 0.6 | < 0.001 |
| LSN MRI T2-w | 2.6 ± 0.6 | 2.2 ± 0.3 | 2.9 ± 0.7 | 0.001 |
| LSN CT-PVP | 2.8 ± 0.6 | 2.4 ± 0.4 | 3.2 ± 0.6 | < 0.001 |
| Spleen length (cm) | 11.6 ± 1.9 | 10.4 ± 1.3 | 12.8 ± 1.7 | < 0.001 |

Unless otherwise specified, data are means ± standard deviations

ALT alanine transferase, AST aspartate transferase, CSPH clinically significant portal hypertension, CT computed tomography, HVPG hepatic venous pressure gradient, LSN liver surface nodularity, MRI magnetic resonance imaging, PVP portal venous phase

^aData are numbers, with percentages in parentheses

^bData in parentheses are ranges

^cThe total exceeds 100% because some patients had more than one cause of cirrhosis

measurements were possible on one or more MRI sequences in three other patients (T1-w-HBP in one patient, T1-w-HBP and CT-PVP in another patient and T1-w-HBP and T2-w in another patient). In the fifth patient, no reliable LSN measurements were possible on T1-w-PVP due to breathing artefacts.

On T1-w-PVP, the LSN score could not be obtained in two of 30 patients (7%) due to breathing artefacts in one patient and limited liver-adipose tissue interface in another patient. On T1-w-HBP, measurements could not be obtained in four of 30 patients (13%) because of limited liver-adipose tissue interface in two patients and limited ascites in two patients. On both T2-w and CT-PVP, two of 30 patients (7%) had LSN measurement failure due to limited liver-adipose tissue interface.

Diagnostic performance of LSN measurements

All CT- and MRI-derived LSN quantifications were correlated with HVPG (CT-PVP: $r = 0.63$, $p = 0.001$, AUROC = 0.908 ± 0.06 ; T1-w-PVP: $r = 0.43$, $p = 0.028$, AUROC = 0.876 ± 0.07 ; T1-w-HBP: $r = 0.50$, $p = 0.012$, AUROC = 0.823 ± 0.08 ; T2-w: $r = 0.51$, $p = 0.007$, AUROC = 0.801 ± 0.09). There were no significant differences in AUROCs in pair-wise comparisons ($p = 0.12$ – 0.88) (Table 2 and Supplemental Table 3).

Compared to CT-based LSN scores, the Bland–Altman plot for MRI T1-w-PVP, T1-w-HBP and T2-w showed a systemic bias of -0.32 [limits of agreement (LOA) of -1.12 and 0.47], -0.14 (LOA of -0.82 and 0.53) and -0.22 (LOA of -0.87 and 0.43), respectively (Fig. 2 and Supplemental Table 4).

CT-based LSN scores were higher in patients with CSPH than in those without (3.2 ± 0.6 vs. 2.4 ± 0.4 ; $p < 0.001$). A cutoff value of 2.62 identified CSPH with a sensitivity of 93% and a specificity of 79%. This cutoff value correctly classified 24/28 (86%) patients.

MRI-based LSN scores were higher in patients with CSPH than in those without on T1-w-PVP (2.7 ± 0.4 vs. 2.2 ± 0.4 ; $p = 0.002$), T1-w-HBP (3.0 ± 0.6 vs. 2.3 ± 0.3 ;

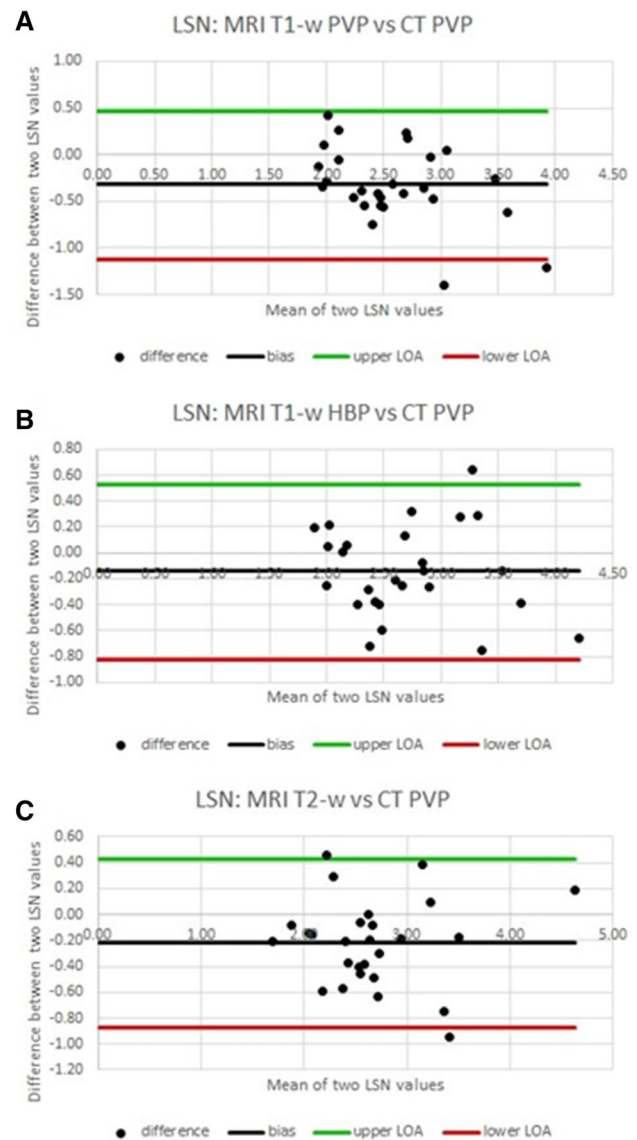


Fig. 2 Bland–Altman plots comparing CT-PVP with MRI T1-w-PVP (a), MRI T1-w-HBP (b) and MRI T2-w (c)

Table 2 Diagnostic performance of CT-based and MRI-based LSN Score

| | R | AUROC | Cutoff value | Sensitivity (%) | Specificity (%) | Positive predictive value (%) | Negative predictive value (%) | No. correctly classified |
|------------------|------|------------------|--------------|------------------|------------------|-------------------------------|-------------------------------|--------------------------|
| LSN CT-PVP | 0.63 | 0.908 ± 0.06 | 2.62 | 92.9 (66.1–99.8) | 78.6 (49.2–95.3) | 81.2 (61.1–92.3) | 91.7 (62.0–98.7) | 24/28 (86%) |
| LSN MRI T1-w-PVP | 0.43 | 0.801 ± 0.09 | 2.24 | 85.7 (57.2–98.2) | 78.6 (49.2–95.3) | 80.0 (58.9–69.4) | 84.6 (59.7–95.3) | 23/28 (82%) |
| LSN MRI T1-w-HBP | 0.50 | 0.876 ± 0.07 | 2.23 | 92.3 (64.0–99.8) | 76.9 (46.2–95.0) | 80.0 (59.4–91.6) | 90.9 (59.8–98.5) | 22/26 (85%) |
| LSN MRI T2-w | 0.51 | 0.823 ± 0.08 | 2.52 | 73.3 (44.9–92.2) | 92.3 (64.0–99.8) | 91.7 (62.0–98.7) | 75.0 (56.1–87.6) | 23/28 (82%) |

AUROC area under the receiver operating characteristics, CT computed tomography, HBP hepatobiliary phase, LSN liver surface nodularity, MRI magnetic resonance imaging, PVP portal venous phase, r correlation coefficient

$p < 0.001$) and T2-w (2.9 ± 0.7 vs. 2.2 ± 0.3 ; $p = 0.001$). For T1-w-PVP, a cutoff value of 2.24 identified CSPH with a sensitivity of 86% and a specificity of 79%. For T1-w-HBP, a cutoff value of 2.23 identified CSPH with a sensitivity of 92% and a specificity of 77%. For T2-w, a cutoff value of 2.52 identified CSPH with a sensitivity of 73% and a specificity of 92%. Table 2 shows an overview of the diagnostic performance of CT- and MRI-based LSN scores.

An MRI-based LSN score could be reliably computed in 3, 2, 1 and 0 sequences in 25 (83%), 3 (10%), 1 (3%) and 1 (3%) patients, respectively. In the 29 patients with at least one reliable MRI-based LSN score, the score was found to be above 3, 2, 1 or no cutoff values in 10 (35%), 6 (21%), 4 (14%) and 9 (31%) patients, respectively. There was a strong association between the number of LSN scores above cutoff values and the presence of CSPH: 8/9 (89%) patients with all LSN scores below cutoff values had no CSPH, while 8/10 (80%) of those with all LSN scores above cutoff values had CSPH ($p = 0.005$). Similar results were found when the analysis was limited to the 25 patients with reliable LSN scores on all MRI sequences (Fig. 3).

Inter- and intra-reader variability

For inter-reader variability, the intraclass correlation coefficient (ICC) for CT-based LSN scores was 0.95 (95% CI 0.88, 0.98). For MRI T1-w-PVP, T1-w-HBP, and T2-w, the ICC was 0.82 (95% CI 0.64, 0.91), 0.87 (95% CI 0.72, 0.94) and 0.95 (95% CI 0.89, 0.98), respectively. The

Bland–Altman plot for CT-based LSN scores showed a systemic bias of -0.04 (LOA of -0.45 and 0.38). For MRI T1-w-PVP, T1-w-HBP and T2-w, the Bland–Altman plot showed a systemic bias of -0.01 (LOA -0.53 and 0.52), 0.10 (LOA -0.47 and 0.68) and -0.01 (LOA -0.44 and 0.43), respectively.

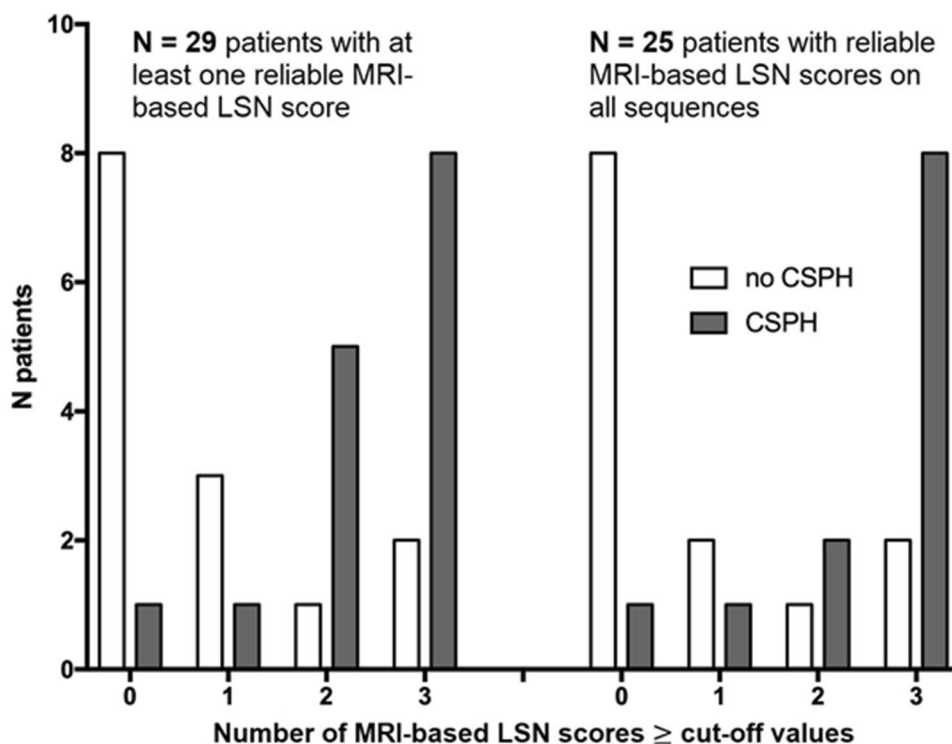
For intra-reader variability, the intraclass correlation coefficient for CT-based LSN scores was 0.92 (95% CI 0.82, 0.96). For MRI T1-w-PVP, T1-w-HBP and T2-w, the ICC was 0.92 (95% CI 0.83, 0.96), 0.95 (95% CI 0.90, 0.98) and 0.89 (95% CI 0.78, 0.95) respectively. The Bland–Altman plot for CT-based LSN scores showed a systemic bias of -0.02 (LOA -0.52 and 0.47). For MRI T1-w-PVP, T1-w-HBP and T2-w, the Bland–Altman plot showed a systemic bias of -0.01 (LOA -0.37 and 0.35), 0.11 (LOA -0.24 and 0.45) and 0.04 (LOA -0.51 and 0.59), respectively.

Supplemental Table 5 shows an overview of intra- and inter-reader agreement.

Discussion

The LSN score is a computer-based quantitative method to measure liver surface nodularity on cross-sectional images that has been shown to be accurate in the diagnosis and staging of liver fibrosis [11–13, 17]. Recently, the performance of this software has been shown to be good for the diagnosis of CSPH in patients with compensated cirrhosis on CT, reflecting the correlation between liver architectural changes

Fig. 3 Bar chart illustrating the association between the number of MRI-based LSN scores above cutoffs and the presence of CSPH



(liver fibrosis and regenerative nodules) and the development of portal hypertension [14, 18]. However, most studies used CT to compute LSN; the application of LSN measurements to MRI images has been reported in two studies to evaluate liver fibrosis alone [15, 19]. The current study shows that MRI-based LSN is also accurate for the detection of CSPH in patients with cirrhosis. It also suggests that the diagnostic performance of MRI-based LSN, especially with contrast-enhanced sequences, is similar to that obtained with contrast-enhanced CT. This has important clinical value since MRI examinations are frequently performed in patients with cirrhosis. The routine use of this rapid, non-invasive technique in association with MR imaging to detect portal hypertension during a pre-surgical workup and patient follow-up could provide valuable clinical information.

It is important to determine which sequences offer the most accurate and reproducible LSN quantification. LSN quantification is based on the presence of significant liver-fat contrast. Thus, we chose to use a non-fat-saturated rather than a fat-saturated T2-w sequence, and pre-contrast non-fat-saturated T1-w acquisitions were initially excluded from the study because of insufficient liver-fat contrast, resulting in the failure of most of the measurements. Overall, one sequence was not found to be significantly better than others. In fact, we believe that one of the advantages of MR imaging is that LSN measurements may be performed on more than one sequence. In particular, we showed that when more than one LSN score could be derived from different sequences, the addition of their individual values increased the likelihood of the presence of CSPH.

The failure rate of CT-based LSN quantification is low, ranging from 0 to 4% in previous studies [11, 12, 14, 15] and consistent with the 7% observed in our CT-PVP images. Lo et al. [15] found a higher failure rate for MRI-based LSN quantification with a T2-weighted LSN score of 32%, which is considerably higher than the 7% observed in our study, and a lower failure rate for the T1-weighted HBP phase LSN score of 0%, which was lower than the 13% observed in our study. Once again, a possible advantage of MR imaging is the acquisition of different pre- and post-contrast sequences. Indeed, if LSN quantification fails with one sequence, this may be compensated for by using another sequence. It is interesting to note that there was only one failure in all the analysed sequences.

Because Gd-BOPTA was used, HBP images could be analysed. In a retrospective study by Lo et al., the diagnostic performance of axial T1-w-HBP for the diagnosis of cirrhosis by LSN quantification was poor, while the performance of coronal sequences was better [15]. The authors hypothesised that this discrepancy might be due to a more well-defined fat plane along the surface of the right lobe than that on the left lobe and also suggested that cardiac artefacts could be more marked in the left lobe and affect

measurements. However, it is difficult to understand why these limitations would affect HBP images only. Moreover, our results do not confirm this observation since the performance with axial HBP images in our study was good. The use of two different liver-specific contrast agents (Gd-BOPTA in the current study and Gd-EOB-DTPA in the study by Lo et al.) could be an explanation. However, hepatic parenchymal enhancement tends to be less impaired with Gd-EOB-DTPA than with Gd-BOPTA in patients with advanced cirrhosis [20].

Indeed, LSN quantification was not affected by the presence of undetected clinically mild perihepatic ascites on CT or with T2- and T1-w-PVP MRI. However, on T1-w-HBP, the presence of perihepatic ascites resulted in LSN measurement failure in a few patients. This may have been due to the relative enhancement of ascites on HBP following the injection of Gd-BOPTA, resulting in a decrease in contrast between the liver and perihepatic fluid [21, 22]. This was not expected to occur after injection of Gd-EOB-DTPA.

Based on the study by Lo et al., ten LSN measurements were selected as the threshold for a valid LSN score, the same number that was used in the studies by Pickard et al. and Besa et al. [12–15]. In the study by Smith et al., eight measurements were the minimum to obtain a valid score, while five measurements were used in the study by Sartoris et al. [14, 23]. No consensus or technical recommendations from the manufacturer are available, and further studies are needed to clarify this issue.

This study has several limitations besides its retrospective design. First, the study population was small. This was due to the strict inclusion criteria which were used to perform inter-method comparisons of LSN quantifications. Thus, studies are needed in large populations to validate these results. Second, we did not evaluate the prognostic value of LSN. This was beyond the scope of the study and shall be addressed in further studies. Third, cutoff values were calculated independently for each MRI sequence and CT examination to determine the best diagnostic performance. A single cutoff value to differentiate patients with or without CSPH must be established in larger studies for the clinical application of this measurement.

In conclusion, MRI-based LSN quantification is accurate and reproducible for the detection of clinically significant portal hypertension in patients with cirrhosis. The diagnostic performance of MRI-based LSN, including measurements extracted from HBP images, is similar to that obtained with contrast-enhanced CT.

References

1. Berzigotti A, Reig M, Abraldes JG, Bosch J, Bruix J (2015) Portal hypertension and the outcome of surgery for hepatocellular

- carcinoma in compensated cirrhosis: a systematic review and meta-analysis. *Hepatology* 61(2):526-536. <https://doi.org/10.1002/hep.27431>.
2. Liu J, Zhang H, Xia Y, et al. (2019) Impact of clinically significant portal hypertension on outcomes after partial hepatectomy for hepatocellular carcinoma: a systematic review and meta-analysis. *HPB* 21(1):1-13. <https://doi.org/10.1016/j.hpb.2018.07.005>.
 3. De Franchis R (2000) Updating consensus in portal hypertension: report of the Baveno III Consensus Workshop on definitions, methodology and therapeutic strategies in portal hypertension. *J. Hepatol.* 33(5):846-822.
 4. Cucchetti A, Cescon M, Golfieri R, et al. (2016) Hepatic venous pressure gradient in the preoperative assessment of patients with resectable hepatocellular carcinoma. *J. Hepatol.* 64:79-86. <https://doi.org/10.1016/j.jhep.2015.08.025>.
 5. Augustin S, Millan L, Gonzalez A, et al. (2014) Detection of early portal hypertension with routine data and liver stiffness in patients with asymptomatic liver disease: a prospective study. *J. Hepatol.* 60(3):561-569. <https://doi.org/10.1016/j.jhep.2013.10.027>.
 6. de Franchis R, Baveno VI Faculty (2015) Expanding consensus in portal hypertension: Report of the Baveno VI Consensus Workshop: Stratifying risk and individualizing care for portal hypertension. *J. Hepatol.* 63(3):743-752. <https://doi.org/10.1016/j.jhep.2015.05.022>.
 7. Elkrief L, Ronot M, Andrade F, et al. (2018) Non-invasive evaluation of portal hypertension using shear-wave elastography: analysis of two algorithms combining liver and spleen stiffness in 191 patients with cirrhosis. *Aliment. Pharmacol. Ther.* 47(5):621-630. <https://doi.org/10.1111/apt.14488>.
 8. Motosugi U, Roldán-Alzate A, Bannas P, et al. (2019) Four-dimensional Flow MRI as a Marker for Risk Stratification of Gastroesophageal Varices in Patients with Liver Cirrhosis. *Radiology* 290(1):101-107. <https://doi.org/10.1148/radiol.2018180230>.
 9. Gouya H, Grabar S, Vignaux O, et al. (2016) Portal hypertension in patients with cirrhosis: indirect assessment of hepatic venous pressure gradient by measuring azygos flow with 2D-cine phase-contrast magnetic resonance imaging. *Eur. Radiol.* 26(7):1981-1990. <https://doi.org/10.1007/s00330-015-3991-x>.
 10. Ronot M, Lambert S, Elkrief L, et al. (2014) Assessment of portal hypertension and high-risk oesophageal varices with liver and spleen three-dimensional multifrequency MR elastography in liver cirrhosis. *Eur. Radiol.* 24(6):1394-1402. <https://doi.org/10.1007/s00330-014-3124-y>.
 11. Smith AD, Branch CR, Zand K, et al. (2016) Liver Surface Nodularity Quantification from Routine CT Images as a Biomarker for Detection and Evaluation of Cirrhosis. *Radiology* 280(3):771-81. <https://doi.org/10.1148/radiol.2016151542>.
 12.) Pickhardt PJ, Malecki K, Kloke J, Lubner MG (2016) Accuracy of Liver Surface Nodularity Quantification on MDCT as a Noninvasive Biomarker for Staging Hepatic Fibrosis. *AJR Am. J. Roentgenol.* 207(6):1194-1199. <https://doi.org/10.2214/ajr.16.16514>
 13. Pickhardt PJ, Graffy PM, Said A, et al. (2019) Multiparametric CT for Noninvasive Staging of Hepatitis C Virus-Related Liver Fibrosis: Correlation with the histopathologic Fibrosis score. *AJR Am. J. Roentgenol.* 212(3):547-553. <https://doi.org/10.2214/AJR.18.20284>.
 14. Sartoris R, Rautou PE, Elkrief L, et al. (2018) Quantification of Liver Surface Nodularity at CT: Utility for Detection of Portal Hypertension. *Radiology* 289(3):698-707. <https://doi.org/10.1148/radiol.2018181131>.
 15. Lo GC, Besa C, King M, et al. (2017) Feasibility and reproducibility of liver surface nodularity quantification for the assessment of liver cirrhosis using CT and MRI. *Eur J Radiol Open* 21(4):95-100. <https://doi.org/10.1016/j.ejro.2017.07.001>.
 16. Neri E, Bali MA, Ba-Ssalamah A, et al. (2016) ESGAR consensus statement on liver MR imaging and clinical use of liver-specific contrast agents. *Eur. Radiol.* 26(4):921-931. <https://doi.org/10.1007/s00330-015-3900-3>.
 17. Lubner MG, Jones D, Said A, et al. (2018) Accuracy of liver surface nodularity quantification on MDCT for staging hepatic fibrosis in patients with hepatitis C virus. *Abdom. Radiol.* 43(11):2980-2986. <https://doi.org/10.1016/j.gtc.2018.04.012>.
 18. Sethasine S, Jain D, Groszmann RJ, Garcia-Tsao G. (2012) Quantitative histological-hemodynamic correlations in cirrhosis. *Hepatology* 55(4):1146-1153. <https://doi.org/10.1002/hep.24805>.
 19. Besa C, Wagner M, Lo G, et al. (2018) Detection of liver fibrosis using qualitative and quantitative MR elastography compared to liver surface nodularity measurement, gadoxetic acid uptake, and serum markers. *J. Magn. Reson. Imaging* 47(6):1552-1561. <https://doi.org/10.1002/jmri.25911>.
 20. Khouri Chalouhi C, Vernuccio F, Rini F, et al. (2019) Hepatobiliary phase in cirrhotic patients with different Model for End-stage Liver Disease score: comparison of the performance of gadoxetic acid to gadobenate dimeglumine. *Eur. Radiol.* 29(6):3090-3099. <https://doi.org/10.1007/s00330-018-5884-2>.
 21. Ciolina M, Di Martino M, Bruno O, et al. (2018) Peritoneal and pleural fluids may appear hyperintense on hepatobiliary phase using hepatobiliary MR contrast agents. *Eur. Radiol.* 28(7):3020-3031. <https://doi.org/10.1007/s00330-017-5261-6>.
 22. Bonatti M, Valletta R, Zamboni G, et al. (2019) Ascites relative enhancement during hepatobiliary phase after Gd-BOPTA administration: a new promising tool for characterising abdominal free fluid of unknown origin. *Eur. Radiol.* 29(6):2830-2836. <https://doi.org/10.1007/s00330-018-5932-y>.
 23. Smith AD, Zand KA, Florez E, et al. (2017) Liver Surface Nodularity Score Allows Prediction of Cirrhosis Decompensation and Death. *Radiology*, 283(3):711-722. <https://doi.org/10.1148/radiol.2016160799>

Publisher's Note Springer Nature remains neutral with regard to jurisdictional claims in published maps and institutional affiliations.